Thermal expansion and mean-square displacements of the Al(110) surface studied with medium-energy ion scattering

B. W. Busch and T. Gustafsson
Department of Physics and Astronomy, and Laboratory for Surface Modification, Rutgers University, 136 Frelinghuysen Road, Piscataway, New Jersey 08854-8019
(Received 6 October 1999)

We report determinations of surface interlayer spacings and vibrational amplitudes of Al(110) in the temperature range 300–660 K, using medium-energy ion scattering with shadowing and blocking. We show that the surface vibrational amplitudes are anisotropic, and present results for their temperature dependence. The in-plane anisotropy changes sign between room temperature and 600 K. We also find evidence for a large mean-square displacement perpendicular to the surface for atoms in the second layer; a result that is quite nonintuitive but has been predicted theoretically. Such a finding also supports a predicted microscopic mechanism for surface premelting where adatoms are formed from displaced atoms in the second layer. Our data also show a smooth expansion of the first interlayer spacing in this temperature range.

I. INTRODUCTION

Al(110), with the open atomic arrangement of fcc(110), has been seen experimentally to go through all the familiar stages of disorder[1] as the temperature is increased toward the bulk melting point, namely, roughening,[2–4] premelting,[3–5] and surface melting.[3–8] This makes it an interesting choice for further studies of surface dynamics and structure at elevated temperatures. Topics include the degree and nature of the surface anharmonicity, and the microscopic mechanism of premelting (the apparent proliferation of adatoms and vacancies prior to formation of a quasiliquid at the surface). Previous kinematical low-energy electron diffraction (LEED) measurements[9] have shown a negative thermal expansion of the first interlayer spacing in the temperature range 40–425 K. This observation is consistent with a force constant model by Ditlevsen and Nørskov[10] provided that the first-to-second interlayer effective force constant is increasing with temperature. Another possible explanation offered was an enhanced anharmonicity in the second layer (perpendicular to the surface) greater than that in the first layer. This would allow second-layer atoms to have large vibrational motions toward the surface, and an increasing temperature would lead to an increasing contraction of the first interlayer spacing. Recently, Marzari *et al.*[11,12] have studied this surface using ensemble density functional theory (eDFT) molecular dynamics (MD). In their picture of this surface, atoms in the second layer have natural channels of oscillation normal to the surface and toward the vacuum. The charge density above the second-layer atoms is quite homogeneous, and the bonds are easily stretched, leaving freedom for the atoms to move back and forth along these channels. Hence, they observe strongly enhanced mean-square displacements (MSD's) of atoms in the second layer perpendicular to the surface. Such an observation seems to be a distinctive feature of this crystallographic orientation. It has been seen before in embedded atom method (EAM) MD simulations on Ni(110) (Ref. 13) and Cu(110),[14,15] and in EAM Monte Carlo simulations on Al(110).[16] However, this effect is much more pronounced on the Al(110) surface in the eDFT-MD studies. As the temperature is increased, the center of mass of the second layer moves outward and hence a contraction of the first interlayer spacing is observed. These same channels of oscillation provide a microscopic mechanism for formation of adatoms. During the MD simulations, atoms from the second layer were seen to make excursions onto the surface, forming adatoms and vacancies. Enhanced perpendicular MSD's in the second layer are then, in this picture, the precursor of the premelting mechanism. An experimental measurement of these vibrational amplitudes at elevated temperatures is an important test of this theory.

Another aspect of the premelting process that is not yet fully understood is the degree of in-plane anisotropy at the onset of surface disorder. Based on a comparison of the temperature dependence of LEED spot intensities on Pb(110),[17] Prince *et al.* suggested that the surface disorders anisotropically, with disordering occurring first along the $\langle 110 \rangle$ rows of atoms. This is indicated by a more rapid decay in intensity (after correction for the Debye-Waller part) of a spot with k vector parallel to the $\langle 110 \rangle$ rows, as compared to a spot with k vector perpendicular to these rows. Approximate (no multiple scattering) LEED spot intensities may be calculated from EAM-MD simulations by introducing an electron probing depth in the expression for the layer-by-layer structure factor. This has been done on Al(110),[18,19] and indeed a similar anisotropy is found if an analysis equivalent to that of Prince *et al.*[17] is performed. However, the larger momentum transfer of a LEED spot with k vector along the $\langle 110 \rangle$ rows as compared to one perpendicular to the rows suggests that this measurement of disorder itself is different for the two directions. If the momentum transfer dependence of the structure factors is included in the calculations, the temperature falloff of the orthogonal k vector spot intensities is very similar, suggesting no anisotropy. With ion scattering, one may probe vibrational anisotropy directly in real space, as has been done on Pb(110),[20] Ag(110),[21] and Cu(100).[22]

The purpose of the present work is to investigate the degree of anharmonicity at the Al(110) surface, and test for the possible negative thermal expansion of the first interlayer

spacing. To this end, we report measurements of the first three interlayer spacings in the temperature range 300–660 K. (The meaning of ''interlayer spacings'' becomes ambiguous after roughening and/or premelting transitions; therefore these values are not measured above ≈ 700 K, where most studies have reported the onset of disorder.) Furthermore, to test the prediction of eDFT-MD for strongly enhanced MSD's in the second layer normal to the surface, and to measure the degree of anisotropy of the in-plane vibrations, we report component resolved (in-plane and out-of-plane) vibrational amplitudes for the first two layers at room temperature and 570 K.

II. EXPERIMENTAL PROCEDURE

Medium-energy ion scattering (MEIS), with channeling and blocking, is a powerful method for determination of the structural and vibrational parameters of a crystalline surface.[23–25] When incoming ions (e.g., 40–200 keV protons) are incident upon a crystalline surface along a major crystallographic direction or row of atoms, they are ''channeled'' into the solid. The deflection of the ions due to the first atoms along a row causes the formation of a ''shadow cone,'' greatly reducing the chance of backscattering from successive atoms along the row. As ions travel through the solid, they continuously lose energy due to electronic stopping. Hence, the energy of an emerging backscattered proton is directly related to the depth of the scattering event. This effect, combined with channeling, gives rise to an energy distribution of the scattered particles that exhibits a ''surface peak'' at an energy that only depends on the scattering angle (the angle away from the incident ion direction) and the masses of the projectile and target. Thermal displacements and reconstructions directly affect this process because they make shadowing less perfect, and more ions are backscattered from the surface region. The area of the surface peak also depends on the direction in which the scattered ions are going. Ions exiting the crystal may be deflected by atoms closer to the surface, ''blocking,'' resulting in a nonmonotonic scattering angle dependence of the surface peak area. The position of such ''blocking dips'' provides a sensitive measure of surface atom displacements. A shift in the position of a blocking dip away from the bulk crystal blocking direction is a direct indication of layer relaxation. Accurate determination of structural parameters (atomic locations and vibrational amplitudes) is accomplished by comparing the angular scattering intensity to Monte Carlo computer simulations[26] for trial structures. Structural and vibrational parameters in the simulations are varied until a good fit to the angular scattering intensity is achieved, as determined by an *R*-factor analysis.[27]

Since scattering cross sections are accurately known for the energy range used (Coulomb scattering with manageable screening), the area of the surface peak may be converted or ''normalized'' into visible atoms per row, or alternatively into visible layers. We determine the normalization factors in the experiment, such as the detector solid angle and the fraction of the incident beam intercepted to measure the ion dose, by calibration with a Pt/Si high-energy ion scattering standard. The fraction of backscattered ions that are neutralized, and therefore cannot be detected by the electrostatic analyzer, is also accounted for. Measured charged fractions of protons exiting from metal surfaces in the MEIS energy range vary from ≈ 0.5 to 0.9.[28–30] This may be measured by use of a surface barrier detector (to detect particles of any charge) in conjunction with a pair of deflection plates in front of the detector (for steering away charged ions so that only the neutrals are detected).

Our ion scattering experiments were carried out with a 40.8 keV proton beam. The surface sensitivity of the MEIS technique is derived from the channeling effect, in which surface atoms deflect the incoming ions away from deeper atoms. An important parameter is the shadow cone radius.[23,24] This is the closest distance ions may approach the second atom along a row in a perfect static crystal. For effective channeling, and hence good surface sensitivity, the shadow cone radius should be substantially larger than the vibrational amplitudes perpendicular to the rows of atoms. The shadow cone radius is proportional to the square root of the target atomic number, and inversely proportional to the square root of the beam energy. For aluminum, with a relatively low atomic number, use of protons with energy below ≈ 50 keV gives good surface sensitivity. In this case, the shadow cone radius is approximately twice the bulk one-dimensional (1D) rms vibrational amplitude at room temperature. We can measure the energy distribution of backscattered ions simultaneously over a 13° range in the scattering plane using a high-resolution electrostatic analyzer in conjunction with microchannel plates and a 2D position sensitive detector.[31,32] The system energy and angular resolutions for ≈ 40 keV protons are ≈ 48 eV and $\approx 0.1°$, respectively.

The sample was electropolished in a solution of perchloric acid and acetic anhydride, and prepared in UHV (base pressure $\approx 2\times 10^{-10}$ Torr) by standard sputtering and annealing cycles until a sharp (1×1) LEED pattern appeared. MEIS backscattering can directly monitor sample cleanliness. Oxygen impurities on the surface gave the most trouble. In a low scattering angle (high cross section) configuration, the sensitivity of MEIS to oxygen is ≈ 0.03 monolayers (ML). This amount of oxygen was not detectable on the surface for approximately five hours after cleaning. Data collection was kept within two hours of cleaning. The sample was heated from the back by a tungsten filament, and a type *K* (Chromel-Alumel) thermocouple fastened near the sample monitored the temperature. The accuracy and stability of this procedure were ± 12 K and ± 2.5 K, respectively.

III. RESULTS

A. Scattering configurations

Figure 1 shows a top view of the Al(110) surface and the three scattering planes (perpendicular to the surface) used in this study. The channeling and blocking directions used within each scattering plane are shown in Fig. 2. Interlayer separations that each scattering configuration is most sensitive to are also shown. For instance, channeling and blocking in the {100} plane is between atoms in the first, third, fifth, etc. layers, or between atoms in the second, fourth, etc. layers. This gives a sensitivity of the blocking profile to the first-to-third and second-to-fourth interlayer separations, denoted d_{13} and d_{24}, respectively. By simulating scattering

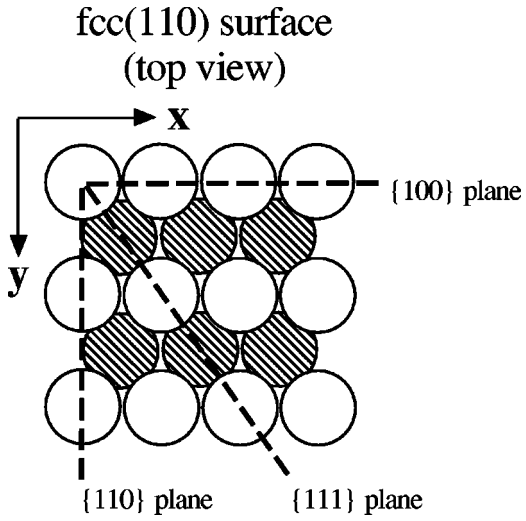

FIG. 1. Top view of the fcc(110) surface showing the three scattering planes (perpendicular to the surface) used in this work. Second-layer atoms are shaded, and the directions denoted *x* and *y* are shown.

data from several configurations simultaneously, one can determine the first several interlayer separations (with $\approx 1-2$ % error in terms of the bulk spacing).

Thermal vibrations of the atoms reduce the shadowing effect and lead to an increase in the scattered yield. In a particular scattering configuration, the vibrational displacements perpendicular to the ingoing and outgoing ion beam directions are probed. Hence, different scattering configurations probe different components of the vibrational amplitudes. An example of this is the contrasting views of the in-plane vibrational amplitudes offered by the configurations in the {100} and {110} planes. An attempt to simulate blocking data from these two configurations simultaneously using only isotropic vibrations leads to a poorer fit than if anisotropic in-plane vibrations are allowed. Figure 3 shows blocking profiles from these two configurations and the best-fit simulations found by optimizing the first three interlayer spacings, but using only isotropic enhanced surface vibrations. In configuration I, the simulated yield over the entire angular range is clearly too low, while in configuration II, the simulated yield is too high. This is seen mainly at the blocking direction near 70°. The simultaneous fit is improved by increasing vibrations in the *y* direction (which raises the overall yield in configuration I), and by decreasing vibrations in the *x* direction (which lowers the overall yield in configuration II). We found a similar in-plane anisotropy on Ag(110) at room temperature.[21] The scattering configuration in the {111} plane (with an incident direction far from normal) provides sensitivity to the perpendicular surface thermal displacements. Use of several incident directions slightly away from the channeling direction (within $\approx \pm 1°$) helps to distinguish between the perpendicular displacements in the first and second layers. The simulation procedure is discussed in detail in a later section.

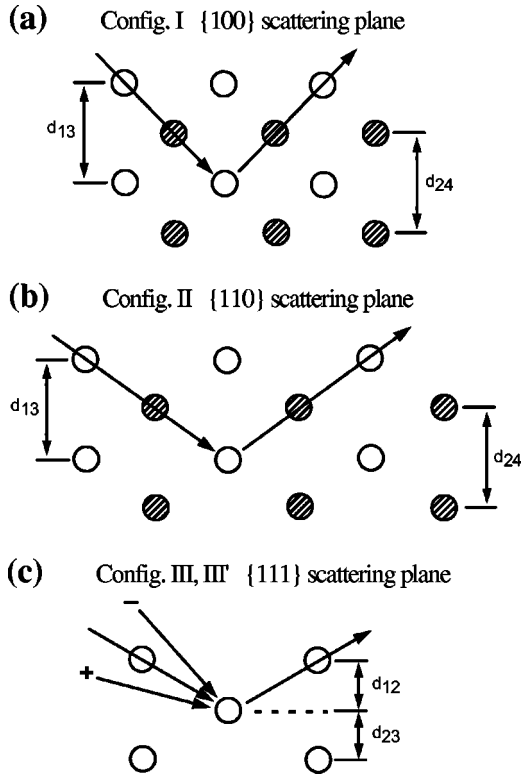

FIG. 2. Channeling and blocking configurations in the three scattering planes of Fig. 1. In (a) and (b), shaded atoms are out of the plane of the page. Interlayer separations for which each configuration is most sensitive are indicated. In (c), configuration III refers to only the channeling direction, while configuration III′ refers to all incident directions. '+' and '−' show the sign convention used for angles away from the channeling direction.

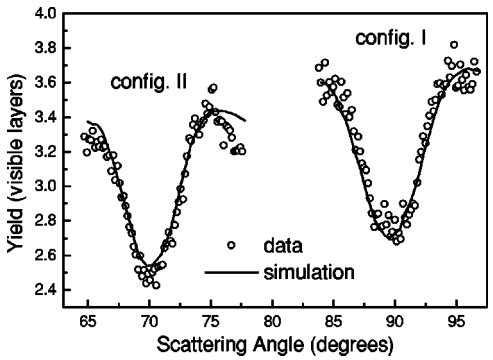

FIG. 3. Plot of angular scattering data or blocking profiles (symbols) from configurations I and II in Fig. 2, along with the best-fit simulations found by optimizing the first three interlayer spacings but using only isotropic vibrations (solid lines). The simultaneous fit can be significantly improved if anisotropic in-plane vibrations are allowed near the surface.

B. Bulk vibrational amplitudes

Ion scattering simulations require bulk vibrational amplitudes as input. Usually this is provided from an independent study or simple model. Previously[21] we reported a method (similar to that used by Frenken *et al.*[33]) where MEIS can be used to determine the bulk vibrational amplitude relative to the Debye model value at room temperature. Such a procedure has been applied to Al(110). Basically, the angular width of the dip in the ion blocking yield from deep within the crystal is sensitive to the bulk vibrational amplitude. Higher vibrational amplitudes reduce the efficiency of shad-

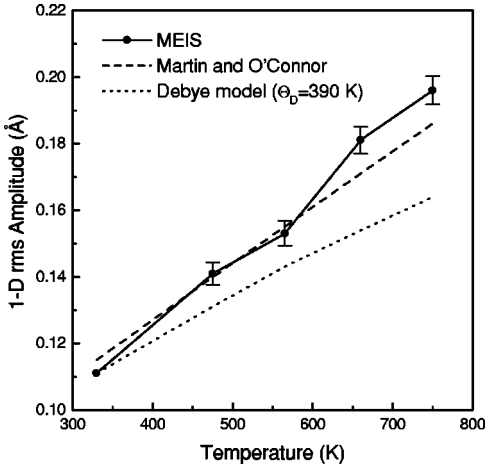

FIG. 4. Plot of the measured bulk vibrational amplitude versus temperature using simulation of ''bulk-scattered'' blocking profiles. A free parameter in the analysis (Ref. 21) was adjusted to make the result agree with the Debye model at room temperature. The x-ray results of Martin and O'Connor (Ref. 34) (solid line), and the Debye model (dashed line) are shown for comparison.

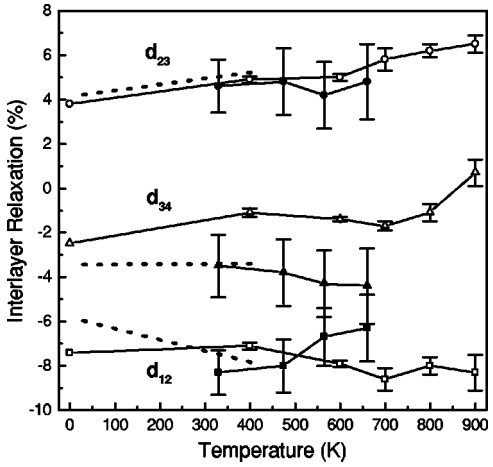

FIG. 5. Temperature dependence of the first three interlayer relaxations (in percent change from the bulk value), as determined from MEIS (closed symbols), LEED (Ref. 9) (dotted lines), and eDFT-MD (Ref. 12) (open symbols).

owing and blocking, and thereby reduce the width of the blocking dip. Comparison of measured bulk blocking yields to an ion scattering simulation in which the bulk vibrational amplitude is varied leads to an experimental measure of this quantity. Since the bulk blocking yield is acquired from a given energy range of scattered ions, a stopping power is needed to translate this energy range to the appropriate depth range in the scattering simulation. The choice of this stopping power (a free parameter in this analysis) is important, because the width of the simulated bulk blocking yield also depends on the depth in the crystal from which the ions scattered. (The width decreases with increasing depth.) This parameter is set by requiring the bulk amplitude to agree with the Debye model value at room temperature. Such an assumption is reasonable since most anharmonic effects are not noticeable at this temperature. For the case of Al, Cu, and several alkali halides, experimental results exist from an x-ray scattering technique for the bulk vibrational amplitudes versus temperature.[34] All show compliance with the Debye result near room temperature. The resulting value for the channeling stopping power is approximately a factor of 2 lower than that for a random direction. This is entirely consistent with theories of channeling,[35] where the stopping power is expected to be smaller in the channels where the electron density is small, and with our previous work on Ag(110).[21]

Figure 4 shows a comparison between the two different experimental results and the Debye model. The error range for the MEIS data is due to a combination of the system angular resolution and 0.1° uncertainty in measuring the full width at half maximum (FWHM) of the blocking profile. Agreement of the two experimental results is reasonable. Together they suggest a significant bulk anharmonicity for Al, which should be taken into account when performing ion scattering simulations of the surface. For instance, use of too low bulk vibrational amplitudes in the simulations will lead to an overestimation of the enhancement of the surface vibrations.

C. Surface thermal expansion and MSD's

Previously we reported the interlayer separations for this surface at room temperature.[36] This work extends these results to the temperature range from 300–660 K. Figure 5 shows our experimental values for the first three interlayer separations in percent change from the bulk value at that particular temperature. These results are obtained from ion scattering simulations of blocking in configurations I, II, and III. The thermal expansion of Al was accounted for, so these results represent relaxations beyond the thermal expansion of the bulk interlayer spacing. Results from Göbel and Blanckenhagen[9] using kinematical LEED and Marzari *et al.*[12] using eDFT-MD are shown for comparison.

Utilizing all of the scattering configurations of Fig. 2, including extra off-channeling directions in the {111} plane, we have found the three components of the vibrational amplitudes in the first two layers at 330 K and 570 K. Table I shows our results normalized to the experimental bulk amplitudes at each temperature. Shown also are calculated results from Marzari *et al.*[12] for temperatures near ours. These values are also normalized to the bulk amplitudes (found in their study) at each temperature.

IV. DISCUSSION

A. Simulation procedure

Monte Carlo ion scattering simulation[26] uses as input the position and vibrational amplitudes of all atoms in the simulated crystal. With some reasonable assumptions, this large set of structural parameters can be reduced to the following 11: three interlayer separations d_{12}, d_{23}, d_{34} (d_{45} and below are fixed at the bulk spacing); six vibrational amplitudes for the first two layers; a third-layer isotropic vibrational amplitude (the fourth layer and below are also isotropic and given by an exponential decay from the third-layer value to the bulk value, with a decay constant of ≈ 1 layer spacing); and lastly, a scale factor (~ 1) applied to simulation output from configurations in the {111} plane where channeling and blocking occur along rows of atoms separated by the nearest-neighbor distance. Such a factor closely approximates the

TABLE I. Component-resolved vibrational amplitudes for the first two layers. See Fig. 1 for the meaning of x and y. Values are given as ratios of the measured 1D rms vibrational amplitudes to the bulk amplitudes (as determined by each technique at each temperature). The averages over both layers of the two in-plane components are also given. Approximate errors for the eDFT and MEIS ratios are ± 0.06 and ± 0.10, respectively.

	T (K)	$x1$	$y1$	$z1$	$x2$	$y2$	$z2$	$(x1+x2)/2$	$(y1+y2)/2$
eDFT-MD	400	1.20	1.52	1.20	1.13	1.03	1.54	1.17	1.28
	600	1.34	1.36	1.23	1.23	1.00	1.47	1.29	1.18
MEIS	330	1.27	1.50	1.23	1.00	1.12	1.12	1.14	1.31
	570	1.53	1.40	1.15	1.34	1.40	1.40	1.44	1.40

effect of vibrational correlations,[37,38] which is an effective decrease in vibrational amplitudes and hence scattering yield. Correlation has been seen to be significant at the surfaces of Al and Ag only for channeling and blocking along nearest-neighbor directions, and at high temperature.[21]

One would like to find the set of structural parameters that will simultaneously optimize the fit of the simulation output to angular scattering data from several scattering configurations. A measure of the goodness of fit (similar to that used previously,[27] and quite standard among MEIS studies) is the following ''R factor'':

$$R(w)=\frac{100}{N}\sqrt{\sum\left(\frac{Y_{data}-wY_{sim}}{Y_{data}}\right)^2}. \qquad (1)$$

Y_{data} and Y_{sim} represent the experimental and simulated angular scattering intensity, respectively. N is the number of points in the sum. This R factor may be used in two different ways. If the scale factor w is set to 1, then the R factor is sensitive to both the overall agreement in yield between the data and simulation, and the agreement in shape (i.e., width and position) of the blocking dip. Alternatively, the scale factor w can be chosen for each trial structure so as to minimize the R factor. Use of such a scaled R factor reduces the sensitivity of the fit to the overall agreement of the absolute yield, and more to fitting of the shape and position of the blocking dip. This scaled goodness-of-fit measure has a special use discussed later. Unless noted otherwise, only the unscaled ($w=1$) R factor is used. A total R factor for a trial structure is found from summing up the above R factors for each scattering configuration.

Optimizing all 11 structural parameters discussed above in all of the scattering configurations simultaneously is computationally prohibitive. However, a divide-and-conquer approach can be developed based on the observations that not all parameters affect the total R factor equally, and that certain subsets of parameters affect the total R factor of different groups of scattering configurations differently. For example, the total R factor is most sensitive to changes in the overall surface vibrational enhancement and the interlayer spacings. One should optimize these first. The details of the anisotropy in the near surface vibrational amplitudes have much less of an effect on the total R factor, but nonetheless the fit can be improved by optimizing these parameters. This set of six parameters can be divided into two subsets; four in-plane amplitudes and two surface-perpendicular amplitudes. Configurations I and II together are sensitive to the in-plane parameters, while the off-channeling configurations labeled III′ are sensitive to the surface-perpendicular vibrations. Neither group of configurations is very sensitive to the other group's corresponding set of parameters, thus uncoupling the set of six vibrational parameters into two manageably sized sets. The sensitivity of configurations I and II to the in-plane vibrational amplitudes was discussed previously in conjunction with Fig. 3. The sensitivity of configuration III′ to the surface-perpendicular amplitudes is illustrated in Fig. 6. Part (a) shows a contour plot of the total R factor (from five incident ion beam directions in the {111} plane) versus the two surface-perpendicular vibrations. Two structures, one near and one away from the minimum, are labeled. Part (b) shows the data for the two extreme off-channeling directions as well as the simulation output for the two structures labeled in part (a). Structure 1 gives a smaller value of the R factor for all five channeling directions separately, and has a clear visual improvement in fit for the $\pm 1.1°$ data.

Based on the above observations, one can find a set of optimum values for these 11 structural parameters using the following procedure.

(1) Starting with a reasonable initial guess for the interlayer spacings, find the best isotropic surface vibrational amplitude in configurations I, II, and III.

(2) Using the scaled R factor in configurations I, II, and III, find the first correction to the interlayer spacings. Use of the scaled R factor uncouples for now the dependence of in-plane vibrational parameters in configurations I and II, and the dependence of the vibrational correlation scale factor in configuration III.

(3) From configurations I and II only, get an overall idea of the in-plane anisotropy by finding separate surface amplitudes (with decay to the bulk value in deeper layers) for the x and y directions, Fig. 1.

(4) Using the above layer spacings and overall in-plane anisotropy, get the correlation scale factor from configuration III′. This is simply the average of the optimum w from the scaled R factor for each channeling direction in configuration III′.

(5) Obtain the second correction (and essentially final values) for the interlayer spacings by using the unscaled R factor for configurations I, II, and III. (III′ may also be included, but this is not necessary since configurations I, II, and III alone are suitably sensitive to the interlayer spacings.)

(6) Determine the in-plane vibrational parameters in configurations I and II only. All four parameters can be opti-

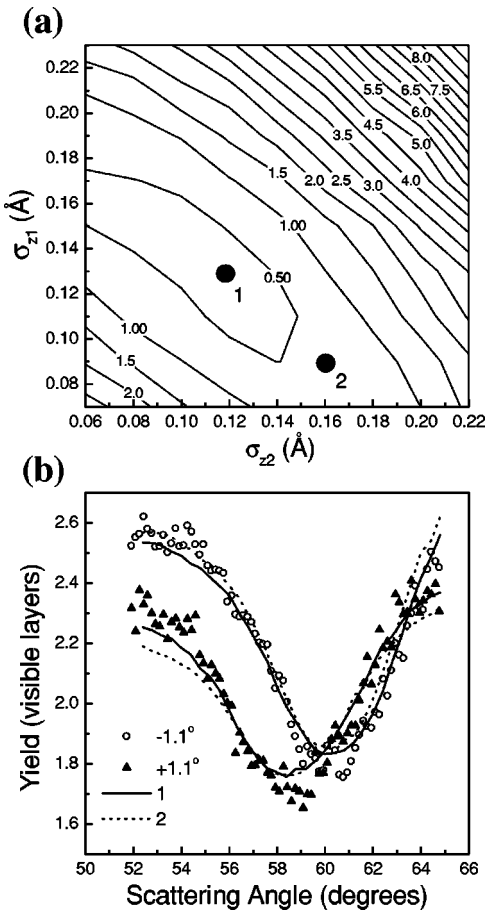

FIG. 6. (a) Contour plot of the total R factor, Eq. (1), from configuration III′ (channeling at 0°, ±0.54°, ±1.1°, and at room temperature) versus the surface-normal 1D rms vibrational amplitudes in the first two layers. Two structures, one near the minimum and one away from the minimum along a direction of gradual change in the R factor, are labeled with large dots. (b) Blocking profiles (symbols) from configuration III′ for off-channeling at ±1.1°, along with the simulation results (solid and dashed lines) for the structures labeled in part (a).

mized simultaneously. There exists some interdependence between the same components in each layer; therefore configurations I and II are more sensitive to the overall in-plane anisotropy than to the relative amount of anisotropy in each layer.

(7) Determine the surface-perpendicular vibrational parameters using configuration III′.

We did not find a change in the results upon inversion of steps (6) and (7), indicating a good independence of these two subsets of the vibrational parameters. Also, to test the order of increasing sensitivity of the total R factor, we made random changes to the final values of the vibrational parameters (consistent with the size of the error bars) but this did not lead to significant changes in reoptimized layer spacings. Errors in the reported results are given by the uncertainty in locating the structural values that minimize the total R factor while varying some subset of the 11 parameters.

An important approximation[26] commonly used in ion scattering simulation is to equate the total hitting and detecting probability (angular yield) of atoms in the crystal to a product of the hitting probability (determined by ingoing ions) and the hitting probability of time-reversed outgoing ions. That is, outgoing ions are simulated as time-reversed ingoing ions with an energy given by the kinematic factor for that scattering angle. Such an approximation essentially neglects correlation between the ingoing and outgoing trajectories, since outgoing ions do not begin from the end point of ingoing ions. This approximation is valid so long as atomic positions do not lie in a region where the ion flux is rapidly changing with position.[26] Such a situation may occur for a very large interlayer relaxation,[39] where deeper atoms are at the edge of the shadow cone of surface atoms. This situation arises in configuration III′, where the incident beam has been misaligned from the channeling direction. An algorithm exists[26] to evaluate the hitting-detecting probability after properly correlating the in-going and time-reversed outgoing tracks. Such a procedure must be applied to scattering simulations of the data in configuration III′.

B. Comparison to eDFT-MD and LEED

Figure 5 shows the temperature dependent interlayer spacings of Al(110) from the previous LEED experiments and MD simulations, and from this work. Overall, these results are in good agreement, lending strong evidence for the validity of the *ab initio* MD approach of Marzari *et al.*[11] The largest disagreement is in the value of d_{34}. It should be noted that d_{45} was included in the eDFT-MD work, where a nearly temperature independent expansion of $\approx 2\%$ was found. Exclusion of this parameter could affect the results of the other parameters in a MEIS study. For example, when a strong oscillatory relaxation exists, neglect of d_{34} in configuration III could lead to a larger contraction being found for d_{12}. In our MEIS study, no substantial effect was found if d_{45} was included because channeling and blocking cause very few ions to scatter from such deep layers. Hence it is a reasonable approximation and simplification to the simulation procedure to ignore it.

Looking more closely at the details of our data, we find no convincing evidence for a negative thermal expansion of the first interlayer spacing. The LEED result yields an expansion coefficient of -24×10^{-6} K^{-1}, with a statistical error of $\approx 10\%$. Such a contraction is not consistent with the eDFT-MD results in this temperature range. At higher temperatures, the MD results show a contraction of d_{12}, explained as the result of a net movement of the second layer outward due to the ''easy'' channel of oscillation. Although the errors are large, the MEIS data suggest an expansion in this temperature range.

Table I summarizes results for the vibrational amplitudes in the first two layers from this work and the eDFT-MD work. For convenience in comparison, and to better visualize the enhancements of vibrations at surfaces, these results are 1D rms amplitudes normalized to their corresponding bulk values for each temperature and technique. Errors for these ratios are about ±0.06 and ±0.10 for the MD and MEIS results, respectively. However, assigning errors to the MEIS results for the in-plane vibrational components is difficult because of the strong interdependence of these parameters (between layers) in calculating the R factor. For instance, a decrease in the x component in layer 1 and a corresponding increase in layer 2 will not always cause a significant change

in the R factor. The scattering technique combined with the simulation procedure outlined above is more sensitive to the overall in-plane anisotropy. More scattering configurations (beyond just I and II) may provide a better discrimination between in-plane vibrational amplitudes in the two layers, as configuration III′ did in the case of the two surface-perpendicular components. Based on these facts, it is probably safer to compare the layer-averaged values of the two in-plane components to the theoretical results. These results are shown in the two right columns of Table I. There is qualitative agreement. However, one aspect of the results in notable agreement is the apparent overall x-y anisotropy reversal as the temperature increases. Such an observation is important because there exists some debate[18,19] on whether the disordering of fcc(110) surfaces is anisotropic, and whether diffraction techniques (sensitive to long range order such as LEED) are able to distinguish an anisotropy from other effects. Also, formation of the surface quasiliquid may proceed via intact parts of $\langle 110 \rangle$ rows moving with liquidlike mobility in the $\langle 110 \rangle$ directions.[6,7] Such a mechanism should be preceded by an enhancement of vibrational amplitudes in the $\langle 110 \rangle$ direction, and hence (since vibrations are usually enhanced perpendicular to the $\langle 110 \rangle$ rows at low temperature) a reversal of the in-plane anisotropy.

An important outcome of the eDFT-MD work is the prediction of large MSD's in the second layer perpendicular to the surface. Such an effect gives a microscopic description of the adatom-vacancy formation process, which in turn may be the necessary precursor to disordering such as premelting and melting. An aim of this work was to measure the vibrational amplitudes in the first two layers perpendicular to the surface. By use of several incident directions in the {111} plane (configuration III′), the interdependence between these two parameters was removed, giving layer-resolved surface-perpendicular MSD's. No evidence for such a large MSD in the second layer is found at room temperature. However, if the temperature is increased to 570 K, we do indeed find that the surface-normal MSD in the second layer increases beyond that of the first layer (Table I). Our room temperature results are consistent with the surface-normal amplitudes reported in previous LEED work,[9] where the second-layer MSD's remained essentially the same as those of the first layer for the entire temperature range studied (30–425 K).

V. SUMMARY

We have used medium-energy ion scattering to investigate the temperature dependent structure and degree of anharmonicity at the Al(110) surface, and to test results from other experimental and theoretical work. We find that there is a slight thermal expansion of the first interlayer spacing from 300–660 K. To test the predictions of eDFT-MD for strongly enhanced surface-normal MSD's in the second layer, we report component-resolved (in-plane and out-of-plane) vibrational amplitudes for the first two layers at room temperature and 570 K. At the higher temperature, we indeed have found evidence for enhanced surface-normal MSD's in the second layer, supporting a predicted microscopic model for surface premelting in which adatoms form as the result of second-layer atoms jumping onto the surface.[12] We also find that as the temperature is increased, the overall x-y anisotropy of the in-plane vibrational components is reversed, beginning with enhanced vibrations perpendicular to the $\langle 110 \rangle$ rows, and ending with enhanced vibrations along the rows. Such an observation is consistent with results of electron diffraction[17] and ion scattering,[20] which support an anisotropic disordering of fcc(110) surfaces. This observation may be the precursor to surface melting via liquidlike mobility of intact $\langle 110 \rangle$ rows.[6,7]

ACKNOWLEDGMENTS

The authors would like to acknowledge the support of this work by the National Science Foundation through Grant No. DMR-9705367. We thank Richard Smith for providing the Al(110) crystal, and Nicola Marzari for valuable discussions.

[1] J. F. van der Veen and J. W. M. Frenken, Surf. Sci. **251/252**, 1 (1991).
[2] M. Schwarz, C. Mayer, P. von Blanckenhagen, and W. Schommers, Surf. Rev. Lett. **4**, 1095 (1997).
[3] H. Dosch, T. Höfer, J. Peisl, and R. L. Johnson, Europhys. Lett. **15**, 527 (1991).
[4] A. Pavlovska, M. Tikhov, Y. Gu, and E. Bauer, Surf. Sci. **278**, 303 (1992).
[5] A. W. D. van der Gon, R. J. Smith, J. M. Gay, D. J. O'Connor, and J. F. van der Veen, Surf. Sci. **227**, 143 (1990).
[6] M. Polcik, L. Wilde, and J. Haase, Phys. Rev. Lett. **78**, 491 (1997).
[7] M. Polcik, L. Wilde, and J. Haase, Surf. Sci. **405**, 112 (1998).
[8] W. Theis and K. Horn, Phys. Rev. B **51**, 7157 (1994).
[9] H. Göbel and P. von Blanckenhagen, Phys. Rev. B **47**, 2378 (1993).
[10] P. D. Ditlevsen and J. K. Nørskov, Surf. Sci. **254**, 261 (1991).
[11] N. Marzari, D. Vanderbilt, and M. C. Payne, Phys. Rev. Lett. **79**, 1337 (1997).
[12] N. Marzari, D. Vanderbilt, A. De Vita, and M. C. Payne, Phys. Rev. Lett. **82**, 3296 (1999).
[13] E. T. Chen, R. N. Barnett, and U. Landman, Phys. Rev. B **41**, 439 (1990).
[14] R. N. Barnett and U. Landman, Phys. Rev. B **44**, 3226 (1991).
[15] L. Yang and T. S. Rahman, Phys. Rev. Lett. **67**, 2327 (1991).
[16] R. J. Smith (private communication).
[17] K. C. Prince, U. Breuer, and H. P. Bonzel, Phys. Rev. Lett. **60**, 1146 (1988).
[18] P. Stoltze, J. K. Nørskov, and U. Landman, Surf. Sci. **220**, L693 (1989).
[19] P. Stoltze, J. Chem. Phys. **92**, 6306 (1990).
[20] A. W. D. van der Gon, H. M. van Pinxteren, J. W. M. Frenken, and J. F. van der Veen, Surf. Sci. **244**, 259 (1991).
[21] B. W. Busch and T. Gustafsson, Surf. Sci. **407**, 7 (1998).
[22] Q. T. Jiang, P. Fenter, and T. Gustafsson, Phys. Rev. B **44**, 5773 (1991).
[23] J. F. van der Veen, Surf. Sci. Rep. **5**, 199 (1985).
[24] W. C. Turkenburg, W. Soszka, F. W. Saris, H. H. Kersten, and B.

G. Colenbrander, Nucl. Instrum. Methods **132**, 587 (1976).
[25] D. S. Gemmell, Rev. Mod. Phys. **46**, 129 (1974).
[26] J. W. M. Frenken, R. M. Tromp, and J. F. van der Veen, Nucl. Instrum. Methods Phys. Res. B **17**, 334 (1986).
[27] I. Stensgaard, R. Feidenhans'l, and J. E. Sørensen, Surf. Sci. **128**, 281 (1983).
[28] G. G. Ross and B. Terreault, Nucl. Instrum. Methods Phys. Res. B **15**, 146 (1986).
[29] R. Behrisch, W. Eckstein, P. Meischner, B. M. U. Scherzer, and H. Verbeek, *Atomic Collisions in Solids* (Plenum Press, New York, 1975), Vol. 1.
[30] J. A. Phillips, Phys. Rev. **97**, 404 (1955).
[31] R. M. Tromp, M. Copel, M. C. Reuter, M. H. von Hoegen, J. Speidell, and R. Koudijs, Rev. Sci. Instrum. **62**, 2679 (1991).
[32] P. M. Zagwijn, A. M. Molenbroek, J. Vrijmoeth, G. J. Ruwiel, R. M. Uiterlinden, J. ter Horst, J. ter Beek, and J. W. M. Frenken, Nucl. Instrum. Methods Phys. Res. B **94**, 137 (1994).
[33] J. W. M. Frenken, P. M. J. Maŕee, and J. F. van der Veen, Phys. Rev. B **34**, 7506 (1986).
[34] C. J. Martin and D. A. O'Connor, J. Phys. C **10**, 3521 (1977).
[35] L. C. Feldman, J. W. Mayer, and S. T. Picraux, *Materials Analysis by Ion Channeling* (Academic Press, New York, 1982).
[36] B. W. Busch and T. Gustafsson, Surf. Sci. **415**, L1074 (1998).
[37] J. H. Barrett and D. P. Jackson, Nucl. Instrum. Methods **170**, 115 (1980).
[38] D. P. Jackson and J. H. Barrett, Nucl. Instrum. Methods Phys. Res. B **2**, 318 (1984).
[39] J. W. M. Frenken, J. F. van der Veen, R. N. Barnett, U. Landman, and C. L. Cleveland, Surf. Sci. **172**, 319 (1986).